J Sol-Gel Sci Technol (2008) 46:259–271
DOI 10.1007/s10971-007-1665-0

ORIGINAL PAPER

Materials doping through sol–gel chemistry: a little something can make a big difference

J.-M. Nedelec · L. Courtheoux · E. Jallot · C. Kinowski · J. Lao · P. Laquerriere · C. Mansuy · G. Renaudin · S. Turrell

Received: 16 August 2007 / Accepted: 26 November 2007 / Published online: 13 December 2007

Abstract Several examples of sol–gel preparation of doped materials are taken to illustrate the various situations where the doping elements are responsible for the main function of the material or govern its structure. Other examples are used to illustrate that sometimes unexpected effects can be observed like structural modification and the appearance of new properties. Rare earth doped scintillators demonstrate higher homogeneity for materials prepared via sol–gel chemistry when compared with classical solid state reaction. The XRD study of rare earth doped orthoborates shows that doping can affect the vaterite to calcite phase transition observed in these compounds. A Raman spectroscopic study has been performed on doped silica xerogels and it has been shown that doping ions can modify greatly the densification process in these amorphous materials. Finally, it has been evidenced that sol–gel chemistry allows the preparation of bioactive ceramics with enhanced properties. In particular Zn-doped HAP with anti inflammatory properties has been prepared and Sr-doped bioactive glasses have demonstrated superior in-vitro bioactivity as evidenced by PIXE-RBS study.

Keywords Doping · Bioceramics · Glasses · Scintillators · Structure · Silica gels · Raman spectroscopy · Hydroxyapatite · Bioactive glasses

J.-M. Nedelec (✉) · C. Mansuy · G. Renaudin
Laboratoire des Matériaux Inorganiques, CNRS, UMR 6002, Université Blaise Pascal, Clermont-Ferrand 2, 24 Avenue des Landais, 63177 Aubiere Cedex, France
e-mail: j-marie.nedelec@univ-bpclermont.fr

J.-M. Nedelec · C. Mansuy · G. Renaudin
Ecole Nationale Supérieure de Chimie de Clermont-Ferrand, 24 Avenue des Landais, 63177 Aubiere Cedex, France

L. Courtheoux · E. Jallot · J. Lao
Laboratoire de Physique Corpusculaire de Clermont-Ferrand, CNRS/IN2P3, UMR 6533, Université Blaise Pascal, Clermont-Ferrand 2, 24 Avenue des Landais, 63177 Aubiere Cedex, France

C. Kinowski · S. Turrell
Laboratoire de Spectrochimie Infrarouge et Raman, CNRS, UMR 8516, Centre d'Etudes et de Recherches Lasers et Applications, Université des Sciences et Technologies de Lille, 59655 Villeneuve d'Ascq, France

P. Laquerriere
Laboratoire de Microscopie Electronique, INSERM – ERM 0203, IFR 53, 1 rue du Maréchal Juin, Reims Cedex 51095, France

C. Mansuy
Synthèse, Structure et Fonctions de Molécules Bioactives, CNRS, UMR 7613, Université Pierre et Marie Curie, 4 Place Jussieu, 75252 Paris Cedex 05, France

1 Introduction

Doping is a very important issue in materials science. Doping corresponds to the deliberate introduction of elements (atoms, ions, molecules, …) in a given material usually to improve its properties. When foreign elements are found in material but not resulting from a controlled procedure, the term impurity is used instead. Many examples can be found in the literature where accidental impurities have revealed themselves to be very good dopants surprisingly enhancing the material properties or bringing new properties. In any case, the study of material doping is a very crucial issue for the production of functional materials. By definition, a doping element is found at a low concentration compared to the main elements of the material typically ranging from a few ppm to a few percent.

In the case of semi-conductors doping can be very low (of the order of 1 doping atom every 100,000,000 atoms) [1]. The higher limit is less well defined but a maximum value of 10–15 at.% could be reasonable.

In many cases the functionality of the material is directly related to doping elements. In some other cases, doping can allow a structural control over the material. Yttrium stabilized zirconia and soda lime glasses are two well known examples related to crystalline and amorphous materials, respectively. Sometimes doping can even induce unexpected effects on the material structure, morphology or functionality.

During the last 30 years, sol–gel processing of materials has been considerably developed. Among the numerous advantages brought by the use of sol–gel chemistry for the preparation of materials, the greater homogeneity obtained by comparison with classical routes is sometimes underestimated. The use of molecular precursors intimately mixed in solution yields definitive homogeneity which is usually conserved throughout the whole process from solution to the final material. As far as doping is concerned, this ability of the sol–gel process to provide materials with a good chemical homogeneity is a very crucial point. Homogeneous doping yields materials with homogeneous properties; this is a fundamental issue for big scale production and low doping levels. As far as doping is concerned, another tremendous advantage of sol–gel chemistry is its high versatility which allows easy variation of the nature of the doping ion and of its concentration easily.

In this paper we will try to give some illustrations of material doping through sol–gel chemistry. In particular we will address the previously mentioned situations:

1. The functionality is directly associated with doping.
2. Doping provides a structural control over the material.
3. Doping provokes unexpected structural modifications.
4. Doping brings new unexpected functionality to the material.

Point 1 will be exemplified with rare earth doped luminescent materials while illustration of 2 will be based upon a study of polymorphism of rare earth doped orthoborates. The Raman spectroscopic study of the influence of transition-metal and rare-earth ion doping on the densification of silica xerogels will illustrate point 3. Finally, recent results obtained on sol–gel derived bioceramics will conclude the paper illustrating point 4.

2 Superior homogeneity in rare-earth doped sol–gel derived scintillators

Luminescent materials are a very good example of materials doping where the function of the material is directly related to the doping ions. Almost all inorganic luminescent materials used commercially result from the association of a matrix (in many cases oxide) and an emitting ion (rare earth or transition metals ion) [2]. In this case, the optical properties of the material come from the doping ion and the undoped material is not even luminescent. The sol–gel process has been widely used for the preparation of luminescent materials but in most of the papers, the main underlined advantage of sol–gel chemistry is the possibility to vary the shape of the phosphor from nanoparticles to micronic powders and thin films.

Research directed towards materials that can convert high–energy radiations (X-rays, γ-rays, neutrons) into UV–visible light, easily detectable with conventional detectors, is in constant development [3, 4]. These materials cover various applications such as medical imaging, high–energy physics and non destructive testing (airport security, industrial control, etc …).

In recent years, we have used the sol–gel process extensively for the preparation of scintillating materials. In effect, the use of molecular precursors is the guarantee of very high chemical homogeneity which is usually also observed in the final material. Furthermore, the high versatility of the sol–gel process makes it possible to obtain various compositions and to vary the nature and the concentration of the doping ion easily. This can not be done usually for single crystal growth. The sol–gel process provides an ideal way to control the level and the homogeneity of doping which is a crucial point for scintillating materials.

From the literature on sol–gel derived scintillators, some conclusions can be drawn. We will take the case of rare earth doped Lu_2SiO_5 (LSO) as an example to illustrate our purpose. LSO is a very efficient scintillator used notably in PET scanners [5, 6].

2.1 Experimental section

A general sol–gel route has been developed for the preparation of scintillator oxides including borates, phosphates and silicates. Detailed procedures can be found in the literature [7]. For LSO, due to the very high reactivity and cost of rare earth alkoxides, we used the in situ preparation of $Lu(^iOPr)_3$ by a metathesis reaction between Lutecium chloride and potassium alcoolate. Tetra Ethyl Ortho Silicate (TEOS) was used as the silicon precursor. Doping was achieved through the same procedure starting with europium, terbium or cerium chlorides. The obtained multicomponent sol was stable and could be used to prepare thin films or destabilized to yield powders [8]. LSO doped with Eu^{3+}, Tb^{3+} and Ce^{3+} ions has been prepared with different doping levels.

The scintillation spectra were recorded with a Jobin-Yvon Triax 320 monochromator coupled with a CCD camera after excitation of the samples with a tungsten X-ray tube working at 35 kV and 15 mA. The signal was collected near the sample with an optical fiber. For estimation of the relative conversion yield estimation, the samples were placed in a quartz tube at a fixed position throughout the measurements. $Bi_4Ge_3O_{12}$ (BGO) and $Gd_2O_2S:Tb^{3+}$ (Gadox) polycrystalline powders were used as a standard for measurements of scintillation yields, of Ce^{3+} and (Eu^{3+}, Tb^{3+}) doped samples, respectively.

2.2 Results and discussion

All materials were carefully characterized by X-ray diffraction, FTIR and Raman spectroscopies confirming the successful preparation of the desired phase Lu_2SiO_5 [9] even for doped samples. At the time of publication [10] this was the first reported study on Eu^{3+} doped LSO. This illustrates the first advantage of sol–gel chemistry for the preparation of scintillating materials, the ease to vary the nature and amount of the doping ions. Clearly, because of segregation it is not possible to prepare LSO:Ce^{3+} crystals by classical techniques at high doping levels. Eu^{3+} or Tb^{3+} doped single crystals are not even reported in the literature. Using the protocol described in section 2.1, and by changing only the starting salt, the sol–gel process allows the preparation LSO doped with various rare earth ions and thus to test new scintillators. The same conclusions can be drawn from our work on lutecium phosphates [11, 12] and borates [13–15]. The measured scintillation yields of Ce^{3+} doped LSO powders are shown in Fig. 1. The best LSO single crystal displays a light yield of 22,500 photons/MeV for a Ce^{3+} doping level of 0.05 at.%. From Fig. 1, it is clear that the optimal doping concentration is shifted towards high values while keeping an equivalent scintillation yield. This is a general observation that has been confirmed with borates, phosphates and other oxides. Quenching concentrations are usually found to be higher for sol–gel derived materials because of better dispersion of doping ions and thus higher average distance between emitting centers.

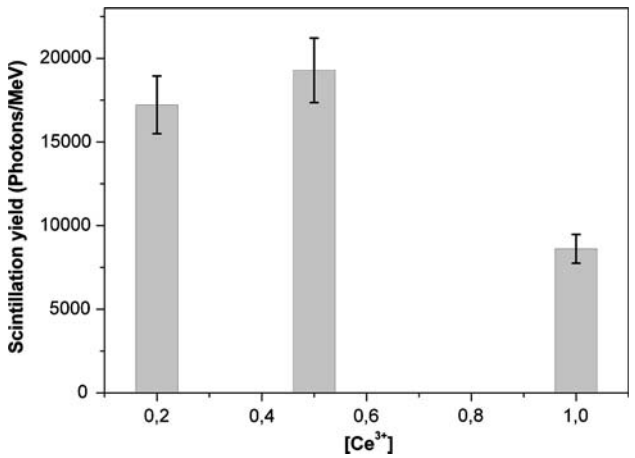

Fig. 1 Evolution of scintillation yield of LSO:Ce^{3+} powders as a function of Ce^{3+} concentration. Quantitative yields have been measured by comparing integrated emission spectra under X-ray excitation with the one of BGO obtained under the same conditions

It is indeed striking to note that optimal doping concentration is usually found much higher for sol-derived materials when compared to solid state derived synthesis. In our opinion, this comes from the conjunction of two opposite effects. The light yield of sol–gel derived materials is usually found to be lower than for the ones prepared by solid state reaction for a given doping level, see [16] for instance. This fact is usually associated with residual hydroxyl groups provoking luminescence quenching. On the other hand, sol–gel derived materials are known to present a better dispersion of doping ions. This allows higher doping concentrations to be reached without concentration quenching and thus higher emission efficiency. These two effects working in opposite directions somehow compensate each other and the optimum light yield is usually found to be equivalent for the different synthesis routes but with different doping levels.

In conclusion, sol–gel chemistry is very valuable for varying the nature of doping ions and thus for trying new scintillating compositions and also for the optimization of doping levels through a better dispersion of doping ions.

3 Control of the structure: polymorphism in rare-earth orthoborates

Rare-earth orthoborates $LnBO_3$ are very interesting matrices for producing luminescent materials upon rare earth doping. The resulting phosphors exhibit good thermal stability and high emission yields. Rare earth orthoborates present three main crystal structures corresponding to the crystal phases of calcium carbonate, aragonite, calcite and vaterite. Some other structures have been observed at high temperatures for $LaBO_3$ [17] and $NdBO_3$ [18]. The phase diagrams of $LnBO_3$ compounds has been established by Levin et al. [19] for Y^{3+} and all Ln^{3+} cations. Because of the high ionic radius of Nd^{3+} and La^{3+}, $NdBO_3$ and $LaBO_3$ exist only in the aragonite form. For YBO_3 and $LnBO_3$ (Ln = Sm–Yb), only the vaterite phase is observed. Lutecium orthoborate $LuBO_3$ is much more interesting from a structural point of view. Because of the small ionic radius of Lu^{3+}, $LuBO_3$ is the only rare earth orthoborate that presents a polymorphism between the vaterite and calcite forms. The low-temperature stable phase is calcite and a phase transition towards the vaterite phase is

observed at 1,310°C. This polymorphism makes $LuBO_3$ a very unique matrix for rare earth doping. Furthermore, because of its high density, (7.4 g cm^{-3} for vaterite and 6.9 g cm^{-3} for calcite), $LuBO_3$ is a very good scintillator when activated with Ce^{3+} or Eu^{3+} ions. In 1999, Boyer et al. [20] proposed a sol–gel route to $LuBO_3$ and observed an inversion of the phase diagram, the vaterite phase being obtained at low temperature (800°C) and a transition towards the calcite phase being observed at 1,100°C. This inversion of the phase diagram for sol–gel derived powders can be explained by considering the initial coordination shell of boron atoms in the alkoxide precursor. The elucidation of this mechanism has motivated our systematic study of the sol–gel preparation of rare earth doped $LuBO_3$.

3.1 Experimental section

The preparation protocol follows the one described in the literature but was been adapted essentially for the annealing conditions (time, temperature). $LuBO_3$ powders doped with Ce^{3+}, Eu^{3+}, Tb^{3+}, Er^{3+} and Yb^{3+} ions at various concentrations were prepared by optimizing the synthesis procedure. This was the first indication of the influence of ion doping on the crystallization of $LuBO_3$. Obviously, since the corresponding borates ($CeBO_3$, $EuBO_3$, $TbBO_3$, $ErBO_3$ and $YbBO_3$) crystallise in the vaterite form, the rare earth substitution of Lu^{3+} ions was made easy even at high doping levels. All powders were calcinated in air at various temperatures in alumina crucibles and characterized by X-ray diffraction on a Siemens D5000 diffractometer working with Cu K_α radiation. When several phases were observed, Rietveld refinements were performed using the program Fullprof.2k Multi-Pattern [21].

3.2 Results and discussion

For an annealing treatment of the amorphous xerogels at 800°C, all samples show only the vaterite phase. For other temperatures, the results obtained show a more complex situation than the one previously described. The first strong discrepancy is the co-existence of two phases vaterite/calcite at temperature as low as 900°C even for undoped samples. Quantitative analysis gives a 76/24% distribution.

Furthermore, the polymorphism of $LuBO_3$ is strongly affected by the nature and the concentration of the doping ion. In particular the temperature of the beginning of crystallization of the calcite phase is variable and the proportion of the two phases is also modified for a given annealing temperature. The influence of doping will be illustrated with two series of samples $LuBO_3$:Eu^{3+} (0–10%) and $LuBO_3$:Ce^{3+} (0–1%). Quantitative analyses of the two phases were performed for various doping levels and various annealing temperatures keeping the annealing time constant. Figure 2 shows the results expressed as the percentage of vaterite phase for the sample doped with europium ions. Clearly for undoped sample, the transformation to calcite begins around 900°C and is completed around 950°C. For doped samples the situation is different, the temperature of appearance of calcite is shifted to 950°C and for the 10% Eu^{3+} sample, the vaterite remains the principal phase even at 1,000°C (76%). Hence, doping with Eu^{3+} ions clearly impedes the transformation to the calcite phase which is delayed to higher temperatures and partially blocked for high doping levels.

The results concerning the Ce-doped series are shown in Fig. 3. Lower doping levels have been studied corresponding to the optimal concentration from a scintillation point of view.

If one considers only extreme temperatures, the doping does not seem to have any effect on the phase transition. Calcite begins to appear in appreciable quantities at 900°C and is the only phase present after annealing at 1,000°C. The data corresponding to the 900°C treatment exhibit a complex behaviour where low doping levels (0.2–0.5%) seem to slightly impede the transformation to calcite whereas the 1% doping strongly favours this transformation (only 35% of vaterite is left at 900°C). The observed presence of mixed oxidation state for cerium (Ce^{3+}/Ce^{4+}) in sol–gel derived materials [7] could partially explain this complex behaviour.

In conclusion, doping with rare earth ions modifies the phase transformation in $LuBO_3$. Different ions can exhibit opposite effects, Eu^{3+} impedes the vaterite to calcite transformation whereas Ce^{3+} seems to accelerate it at least

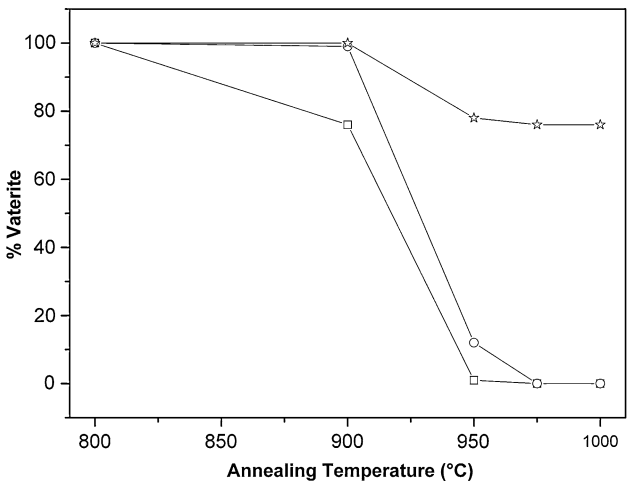

Fig. 2 Percentage of vaterite (%V) in $LuBO_3$:Eu^{3+} samples as determined from Rietveld analysis of powder X-ray diffraction patterns. The percentage of calcite can be deduced from %C = (1 − %V). ($LuBO_3$ –□–, $LuBO_3$:Eu^{3+} 1% –○–, $LuBO_3$:Eu^{3+} 10 % –☆–)

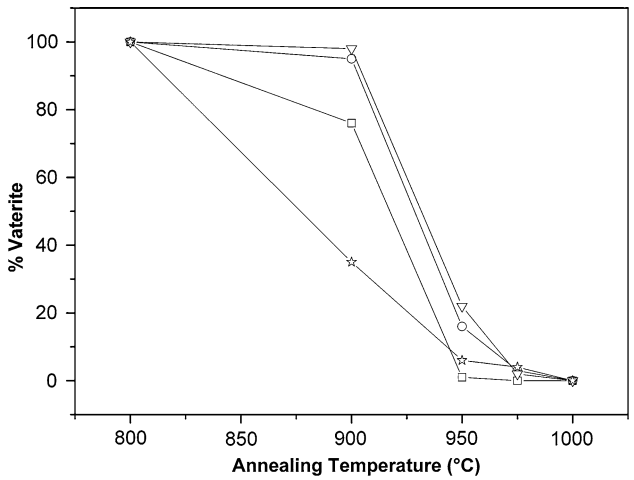

Fig. 3 Percentage of vaterite (%V) in $LuBO_3:Ce^{3+}$ samples as determined from Rietveld analysis of powder X-ray diffraction patterns. The percentage of calcite can be deduced from %C = (1 − %V). ($LuBO_3$ –□–, $LuBO_3:Ce^{3+}$ 0.2% –○–, $LuBO_3:Ce^{3+}$ 0.5% –△–, $LuBO_3:Ce^{3+}$ 1% –☆–)

in the first steps around 900°C. This is a fundamental issue because obviously the optical properties of the phosphor depend strongly on its structure. The vaterite and calcite phases exhibit very different symmetry (space group $P6_3/m$ for vaterite and $R\bar{3}c$ for calcite). This results in different emission features for the substituting ions like radiative lifetime, multiplicity, peak positions and emission yield. By controlling the amount of the phases (both temperature and doping ion dependant) it is possible, to some extent, to tune the emission of the material. Furthermore, because the luminescent ions have an effect on the structure of the borate, using different doping ions (with their corresponding emission characteristics) a more complex tuning could be achieved. Considering finally the difference in the high–energy absorption of the vaterite and the calcite, these aspects open the possibility to prepare scintillating materials with tailored emission properties for specific applications.

4 Unexpected modification of the structure: doping in silica xerogels

The densification process of silica gels has been the object of many studies. A great deal of work has been devoted to the study of the structural changes occurring at various stages of the gel-to-glass transformation as well as to the comparison of the structure of gel-derived glasses and glasses prepared by the conventional melting technique [22, 23]. Most of these studies concerned silica gels and gel-derived silica glasses owing to their potential applications in various areas (coating, optics, …). Transition metal and rare earth ions have been generally used in glasses for their luminescence properties or as probes to follow the structural evolution of the host matrix as a function of annealing temperature or sintering atmosphere [24, 25]. The majority of these studies assumed that probes, whether transition metal or rare earth ions [26, 27], do not modify the gel structure when they are incorporated into the gel in small amounts.

Raman spectroscopy has proven to be a very powerful tool to study the structural evolution of gels and gel-derived glasses. In the following we will summarize the results we have obtained using Raman studies of the densification of doped silica gels.

4.1 Experimental section

Various doped silica gels have been prepared following procedures reported elsewhere [28].

Briefly monolithic silica gels were obtained by hydrolysis/condensation of TEOS in acidic medium. The gels were partially densified by heat treatment at 800°C in air yielding cylindrical mesoporous silica xerogels. These xerogels were finally impregnated with a 0.05 M metallic salt solution before final annealing at temperatures ranging between 800 and 1,150°C.

Densities of the samples were measured by performing mass-to-volume ratios. Weights were measured with an accuracy of $\pm 2.10^{-4}$ g, while micrometer measurements of diameters and thicknesses have an accuracy of ±0.01 mm.

Right-angle Raman measurements were obtained with a triple-monochromator (Dilor T800) using the 514.5 nm line of an Argon-ion laser as an excitation source with a typical power of 300 mW. The signal was detected with a cooled photomultiplier (Thorn EMI). The spectral range investigated was 4–1,200 cm^{-1}, with a spectral slit width of 1 cm^{-1}. For quantitative analysis, spectra were baseline corrected and band decomposition was undertaken. The number and positions of the components for each band were chosen in the same manner as described previously [29]. The spectral bands of interest were the D1 and D2 bands (see below), the *v* Si–OH and finally, the broad band around 430 cm^{-1} which is associated with network Si–O–Si bending vibrations.

4.2 Results and discussion

4.2.1 Density measurements

Upon heating, silica gels experience a densification process, the ultimate step being the transformation into dense glass. From a macroscopic point of view this process is

very well illustrated by the evolution of the density of the material as a function of the annealing temperature (or annealing time at a given temperature). The evolution of the densities of undoped and Ag^+ and Ce^{3+} doped silica gels is displayed in Fig. 4. Starting from a density around 0.90 g cm^{-3}, the gels densify upon heat treatment to reach a plateau around 2.00 g cm^{-3} a little lower than the value of dense amorphous silica (2.20 g cm^{-3}). The behavior of the Ce^{3+} doped samples follows mainly the one of undoped sample, with full densification being reached at 1,050°C. On the other hand, the final density value of 2.00 g cm^{-3} for Ag^+-doped samples is attained for an annealing temperature of only 950°C.

From a macroscopic point of view, the doping with Ag^+ ions has a great effect on the densification process of silica gels. A more detailed study has been performed by Raman spectroscopy.

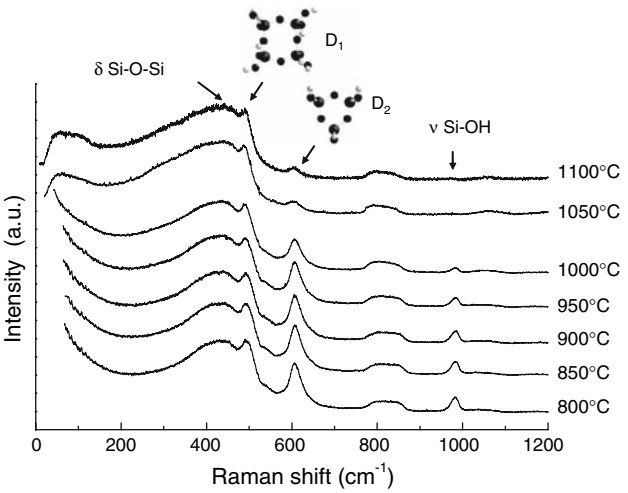

Fig. 5 Raman spectra of undoped silica xerogels annealed at various temperatures. The main bands cited in the discussion are labelled

4.2.2 *Raman spectroscopy measurements*

Raman spectra were collected for all samples, undoped, Ce^{3+} and Ag^+ doped and annealed at various temperatures.

The main structural evolutions of the gels network are illustrated in Fig. 5 where the Raman spectra of an undoped sample are presented.

We observe a progressive decrease of the intensity of the silanol band (ν Si–OH around 980 cm^{-1}) with respect to the intensity of the δ Si–O–Si band around 430 cm^{-1}.

This corresponds to the condensation reaction between silanol groups to form the siloxane backbone. The silanol band is thus a very good indicator of the densification state of the gel.

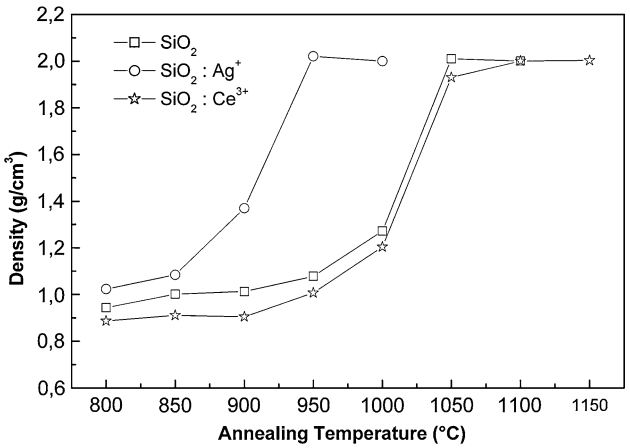

Fig. 4 Evolution of the densities of silica xerogels as a function of the annealing temperature. (undoped xerogels –□–, Ag^+-doped xerogels –○– and Ce^{3+}-doped xerogels –☆–)

The intensities of the sharp bands at 490 and 606 cm^{-1} vary continuously with heat-treatment when compared to that of the 430 cm^{-1} band.

These sharp bands observed in vitreous silica (v-SiO_2) at 490 and 606 cm^{-1} were first tentatively related to network defects and labelled D1 and D2, respectively. Galeener et al. [30, 31] and more recently Barrio et al. [32] assigned the D1 band to the symmetric breathing mode of regular 4-membered silica rings, due to a movement of oxygen atoms. The D2 band was assigned to a similar motion of 3-membered planar rings.

The intensity of the D1 band decreases continuously with temperature up to 1,150°C, This variation indicates that fourfold rings initially present in the wet gel network, are gradually destroyed up to 1,150°C. The intensity of the Raman D2 band first increases up to an annealing temperature of about 950°C and then decreases sharply in agreement with previous works [33].

Finally, in the low-frequency region, a band appears around 40 cm^{-1} for annealing temperature above 1,000°C. This band called "Boson peak" is characteristic of the glassy structure and of a certain medium range order [34]. This region will not be discussed here but a detailed study of the effect of doping on the medium range order of silica xerogels can be found in the literature [35].

Now that the spectral modifications accompanying the densification of undoped gel have been reviewed, we can have a closer look at the effect of doping on this process. Figure 6 presents the evolutions of the normalized intensities of the main Raman bands for an undoped gel, and for Ce^{3+}- and Ag^+-doped silica gels as a function of the annealing temperature.

Silver ions tend to destabilize D1 and D2 rings as attested by Fig. 6a and b where the massive destruction of

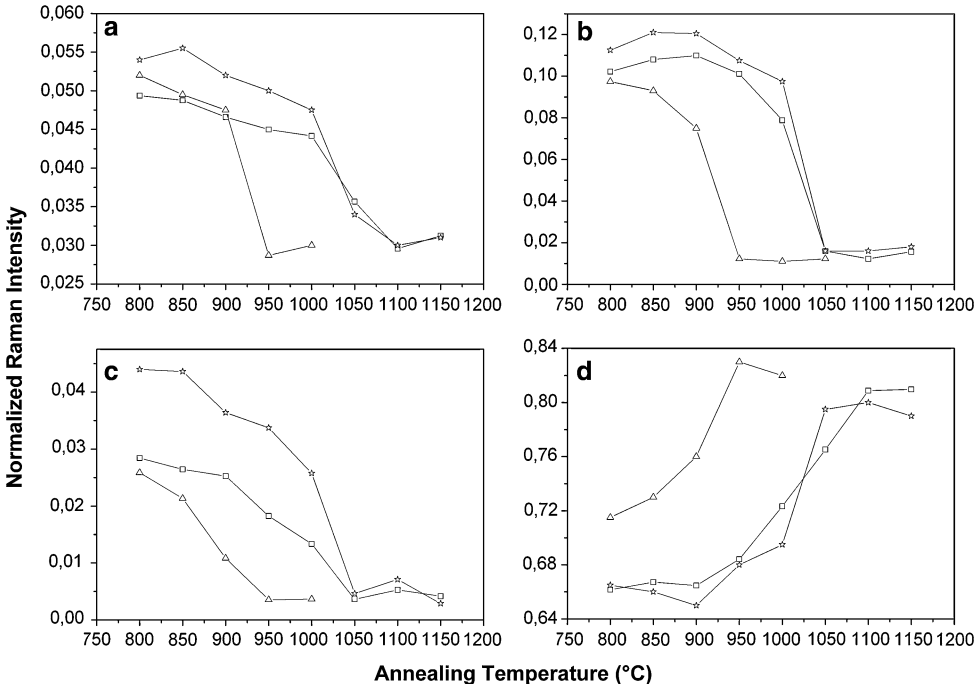

Fig. 6 Evolution of the normalized intensities of the main Raman bands for undoped (–□–) Ag^{+}-doped (–Δ–) and Ce^{3+}-doped (–☆–) samples as a function of annealing temperature. Figure 6a D1 band, Fig. 6b D2 band, Fig. 6c *v* (Si–OH) and Fig. 6d *δ* (Si–O–Si)

4- and 3-membered rings begins at lower temperature compared to undoped sample. The decrease of the intensity of the silanol band also begins at lower temperatures (Fig. 6c) with the concomitant increase of the Si–O–Si band (Fig. 6d). All these observations indicate an acceleration of the densification process of silica upon doping with Ag^{+} ions.

For Ce^{3+} doped samples, the effect seems to be exactly reversed. In effect for any given temperature the intensity of the D1 and D2 bands is higher for Ce-doped samples than for undoped ones (Fig. 6a and b). The same observation is true for the silanol band (Fig. 6c). Doping with Ce^{3+} ions consequently slows down the densification process by stabilizing 3- and 4-membered rings and limiting the condensation of silanol groups.

A similar study has been performed as a function of annealing time for a given annealing temperature [36]. This kinetic study of densification leads to the same conclusion on the role of silver and cerium ions. In a previous work [35, 37] it had been shown that Mn^{2+} ions also slow down the densification process even for very low concentrations (500 ppm).

In conclusion, doping with metal ions greatly affects the densification process of silica gels. Some cations can unexpectedly accelerate the densification while others can slow down the process. Recently Cd^{2+} and Pb^{2+} cations have been shown to slow down the densification in silica gels [38]. Ce^{3+} and Er^{3+} ions have been shown to hinder the densification process in aluminosilicate waveguides [39] but also at the same time to favor the crystallization in this material. Various other cations have been studied and but no clear correlation could be drawn. More classical effect of doping elements on the free volume of silica glass through coordination of metal ions by non bridging oxygens, well established in glass technology, could not be hold responsible for the phenomenon because of the very low doping level involved in our case. Recently Berrier et al. proposed to consider the ionic field strength around the doping cation to predict its effect on the densification of silica gels [40]. Some catalytic effect has also been observed but in hybrid organic–inorganic silica gels where the doping metal ions could catalyze the decomposition of organic groups [41]. Here again, the metal ion concentration were considerably higher than in our case.

In any case for a given annealing procedure (time, temperature and atmosphere) the final structure of the material can differ greatly. This fact has to be taken into account for discussing the physical properties (optical for instance) of the resulting doped materials.

5 Unexpected properties: sol–gel derived bioactive ceramics

Considering the ageing of the population, the future needs in Public Health of developed countries will increase tremendously in the next years, in particular considering the needs for bone substitutes. Historically the function of biomaterials has been to replace diseased or damaged tissues. First generation biomaterials were selected to be as bio-inert as possible and thereby minimize formation of scar tissue at the interface with host tissues. Bioactive

ceramics provide an interesting alternative where an interfacial bonding between the implant and host tissues takes place. These materials induce a specific positive response from the tissue cells and it is even possible to turn on the regeneration process.

Since bone is composed mainly of collagen fibers and hydroxyapatite (HAP) crystals, a lot of attention has been focussed on the later as bone substitute or as a bone engineering scaffold.

The first synthetic bioactive material was discovered in 1969 by Hench and co workers [42]. It is a four component glass which is now commercially used under the name Bioglass®.

These two materials, HAP and Bioglass, and the derivation they inspired, have been the subject of many publications and constitute the references of bioactive ceramics [43–46].

The sol–gel process can be used to prepare these materials and as already mentioned by Li et al. [47], sol–gel derived bioglasses exhibit an extended domain of bioactive composition.

The possibility to combine sol–gel chemistry with template approaches allows the preparation of porous bioceramics with tailored porosity. The bioactivity being related to a kinetic modification of the surface of the ceramics after interaction, this issue is crucial. Furthermore, some trace elements are found in natural bone and some of them are known to be involved in the osteoblast differentiation and bone mineralization. During the last 4 years, we have been focusing our attention on the sol–gel preparation of doped bioceramics (HAP and bioactive glasses) [48, 49].

Once again, the sol–gel process appears to be an ideal route for the controlled doping of materials. In the following we will present the effect of doping in two systems: Zn doped hydroxyapatite and Sr doped bioactive glasses.

5.1 Zn-doped hydroxyapatite

Hydroxyapatite (HAP) is widely used as biomaterials to fill bone defects or to coat metal parts of prostheses. The early dissolution of the amorphous phase of the coating during the bone remodelling leads to the release of calcium phosphate particles having various characteristics and compositions [50, 51]. It has been demonstrated that the interaction between HAP particles and human monocytes led to the release of inflammatory cytokines such as Tumor Necrosis Factor alpha (TNF-α), Interleukin 6 (IL-6) [52] or Interleukin 18 (IL-18) [53] and metalloproteinase. Anti-inflammatory cytokines like Interleukin 10 (IL-10) are also produced [52] and it was shown to inhibit IL-6 and TNF-α production following phagocytosis of polymethymetacrylate particles by monocytes/macrophages [54].

To decrease the inflammatory reaction induced by the phagocytosis of HAP particles, we have elaborated zinc-substituted hydroxyapatite using sol–gel chemistry for the following reasons:

- Zinc is naturally present in bone.
- It has been demonstrated that zinc stimulates bone growth and bone mineralization [55].
- Zinc has a direct effect on osteoblastic cells in vitro [56] and a potent inhibitory effect on osteoclatic bone resorption [57].
- Zinc is also known to modify the production of cytokines [58].
- Zinc-substituted HAP exhibits a modified in vitro bioactivity [59].

In the following section, we will focus on the effect of the zinc concentration on the inflammatory reaction. In a previous paper the down regulation by IL-10 of the inflammatory reaction and the chemotaxis process (i.e. Interleukin 8 (IL-8) production) were also investigated [60].

5.1.1 Experimental section

HAP powders doped with Zn have been prepared following a procedure detailed in [60]. Zn concentration (% Zn/(Ca+Zn)) of 0.5, 1, 2, 5% were obtained.

THP-1 human monocytes were used to evaluate cytokines synthesis. Experiments were made in triplicate. THP-1 were exposed to LPS (1 μg ml^{-1}) (Sigma, USA) as a positive control and to evaluate the effect of zinc-substituted HAP on stimulated cells.

5.1.2 Results and discussion

Characterization of HAP powders: The nominal chemical composition of the hydroxyapatite powders was confirmed by ICP-AES (Inductively Coupled Plasma-Atomic Emission Spectrometry). The nature of the crystal phase was determined by powder X-ray diffraction (XRD) using a monochromatic Cu K_α radiation. X-ray diffraction patterns exhibited the peaks corresponding to hydroxyapatite. A small amount of tricalcium phosphate was also observed.

TNF-α production: THP-1 cells were incubated with the different Zn-doped HAP particles for 6 and 24 h. After 6 and 24 h, the level of TNF-α protein was not detected in control cells (Fig. 7a). Using LPS, the production of TNF-α was maximal at both 6 and 24 h. The production of TNF-α by THP-1 increased when cells were exposed to undoped HAP and zinc-doped HAP particles. But the production

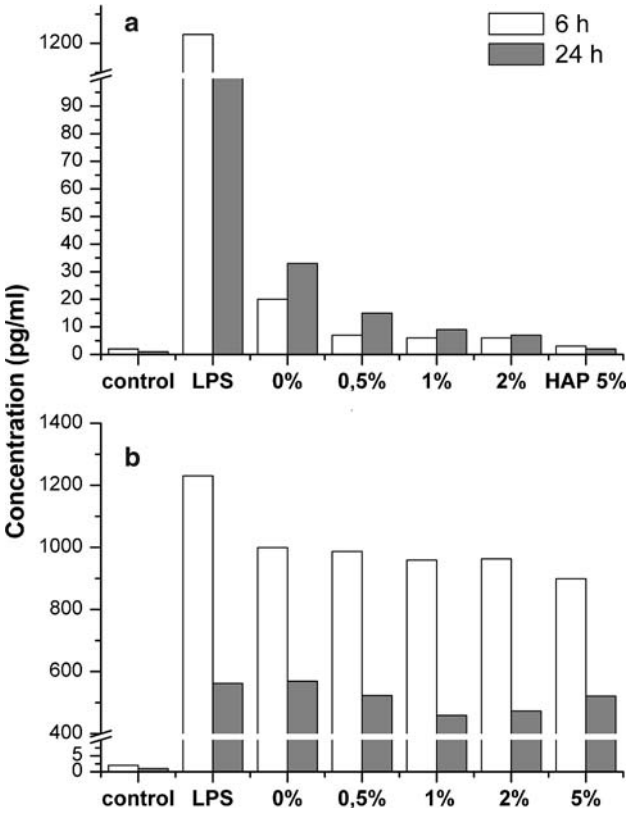

Fig. 7 (**a**) production of TNF-α by THP-1 exposed to zinc-doped HAP particles for 6 and 24 h. (**b**) production of TNF-α by LPS-stimulated THP-1 exposed to zinc-doped HAP particles for 6 and 24 h

induced by the particles remained 20 times less than the production induced by LPS. Due to the low production of TNF-α induced by the HAP particles, cells were stimulated with LPS to investigate the influence of the concentration of zinc on TNF-α production (Fig. 7b). The addition of undoped HAP particles to THP-1 stimulated by LPS increase the production of TNF-α at both 6 and 24 h. But using zinc-doped HAP particles, the production of TNF-α did not change compared to cells stimulated with LPS without any HAP particles.

So the presence of undoped HAP particles increases slightly the production of TNF-α by THP-1. The presence of zinc-doped HAP particles slightly decreased the production of TNF-α by un-stimulated cells.

Effect of HAP particles on IL-1β production: Using the same interaction protocol, the production of another inflammatory cytokine, IL-1β was studied. The presence of HAP particles did not modify the production of IL-1β by non-stimulated THP-1. But the production of IL-1β by LPS-stimulated THP-1 was increased by addition of undoped HAP particles and it decreased when zinc-doped HAP was used.

Effect of HAP particles on IL-6 production: The role of HAP particles on the production of IL-6 by THP-1 and LPS-stimulated THP-1 was then investigated. In summary, undoped HAP or zinc-doped HAP particles did not modify the production of IL-6 by stimulated or non-stimulated THP-1 except for the 5% doped HAP for which the IL-6 production was decreased.

In conclusion, zinc-doped hydroxyapatite has an effect on the production of cytokines by human monocytes cells. The production of TNF-α by non-stimulated cells decreased with the zinc concentration. Using LPS-stimulated cells, the production of IL-1β and IL-6 decreased when zinc-doped HAP particles were used. Hence, Hence, zinc decreases the inflammatory reaction to HAP [61].

5.2 Sr-doped bioactive glasses

Osteoporosis is a very severe disease occurring mainly for old patients (>60) and particularly for women. It results in an important decrease in bone density. Fractures connected to osteoporosis practically doubled in number in the last decade and it is considered that 40% of the women above 50 years old will have an osteoporotic fracture during their lifetime.

Recent studies have shown that oral ingestion of strontium salt can reduce the risk of fracture for osteoporotic patients [62, 63]. The strontium improves the mechanical properties of the bone [64] and has an influence on the solubility of apatites. Strontium favours bone formation through a positive action on osteoblast differentiation and also inhibits bone resorption through negative action on osteoclasts. Furthermore, it allows to have a better link with surrounding tissues. Despite these observations, very few studies have been devoted to Sr-substituted bioceramics. We recently explored the possibility of preparing bioactive glasses doped with strontium by sol–gel chemistry. Preliminary results concerning the in vitro bioactivity of these materials will be described in the following section.

Undoped and Sr-doped bioactive glasses have been prepared in a binary SiO_2−CaO system. Interactions of these materials with physiological fluids have then been studied and the physico-chemical reactions occurring at the surface of the glasses have been examined using Particle Induced X-ray Emission (PIXE).

5.2.1 *Experimental section*

Preparation of the bioactive glass samples: Gel–glass powders containing 75 wt% SiO_2−25 wt% CaO and 75 wt% SiO_2−20 wt% CaO–5 wt% SrO were prepared using the sol–gel process. Tetraethylorthosilicate and calcium nitrate (and Strontium nitrate for doped glass) were mixed in a solution of ethanol in presence of water. The prepared sol was then transferred to an oven at 60°C for gelation and aging. Four hours later, the obtained gel was

dried at 125°C for 24 h, then finally reduced to powder and heated at 700°C for 24 h.

In vitro assays: The glass powders were immersed at 37°C for 15 min, 1, 6 h and 1, 2, 3, 4 days in a standard Dulbecco's Modified Eagle Medium (DMEM, Biochrom AG, Germany), whose composition is almost the same as human plasma. 10 mg of gel–glass powder samples were soaked with a surface area to DMEM volume ratio fixed at 500 cm^{-1}. After interaction, the samples were removed from the fluid, air dried and embedded in resin (AGAR, Essex, England). Before characterization, 1,000 nm thin sections of the glass powder samples were prepared by means of a Leica EM UC6 Ultramicrotome, and laid out on 50 mesh copper grids. The sections and grids were then placed on a Mylar film with a hole of 3 mm in the centre.

PIXE-RBS analysis: Analyses of the biomaterial/biological fluid interface were carried out using nuclear microprobes at CENBG (Centre d'Études Nucléaires de Bordeaux-Gradignan, France). For PIXE analyses, we chose proton scanning micro-beam of 1.5 MeV for undoped sample and 2.9 MeV for doped sample and 100 pA in intensity. The beam diameter was about 1 μm. An 80 mm^2 Si(Li) detector was used for X-ray detection, orientated at 135° with respect to the incident beam axis and equipped with a beryllium window 12 μm thick. PIXE spectra were treated with the software package GUPIX. Relating to RBS, a silicon particle detector placed 135° from the incident beam axis provided us with the number of protons that interacted with the sample. Data were treated with the SIMNRA code.

5.2.2 *Results and discussion*

Elemental maps for each immersion time in DMEM were recorded by PIXE-RBS. Figure 8 a, b, and c represent the elemental distribution of Si, Ca and P, respectively for an undoped glass after 15 min of interaction with biological fluids. The grain reacts very quickly since some phosphorus coming from the solution is already integrated into the periphery of the material (Fig. 8c). After 1 h soaking, we

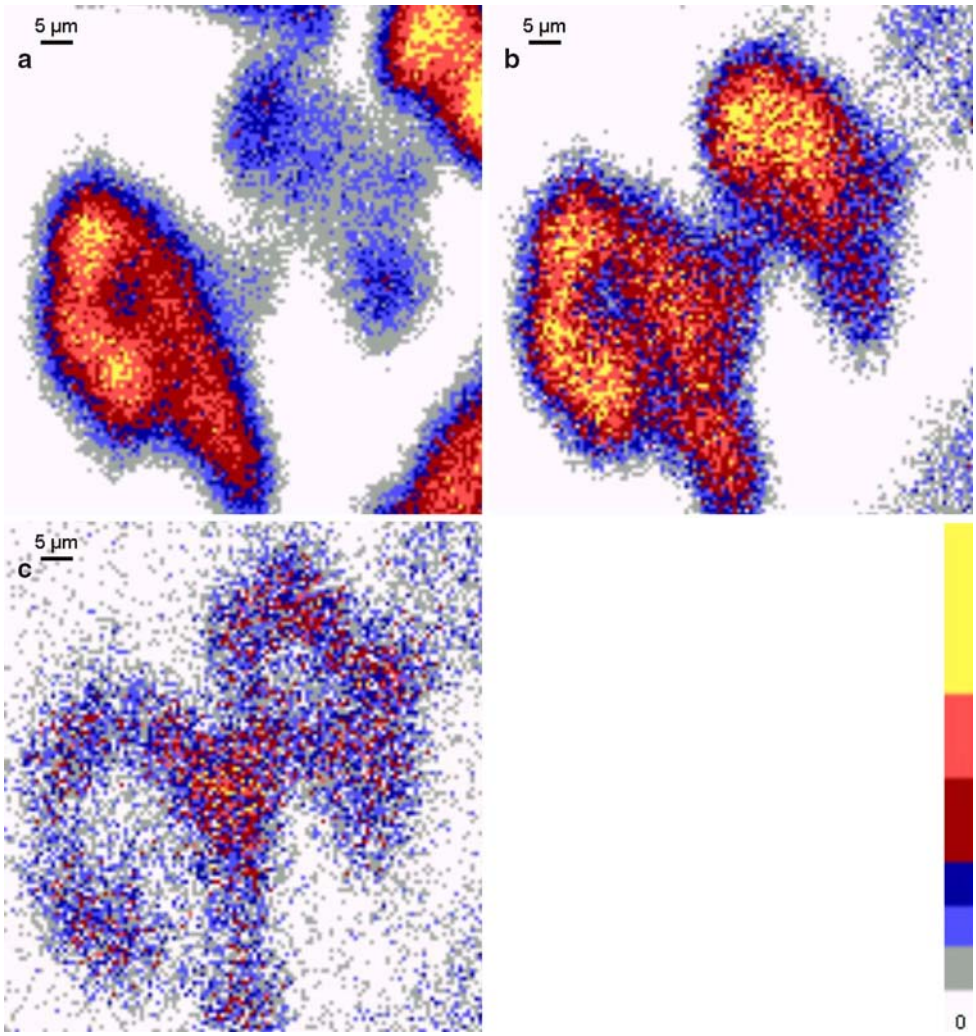

Fig. 8 PIXE elemental maps of a 75 wt% SiO_2–25 wt%CaO glass after 15 min. of interaction with biological fluids. (**a**) Silicon, (**b**) calcium and (**c**) phosphorus

note that calcium has clearly diffused from the glass (Fig. 9b). Ion exchange between the grains and the solution has occurred and traces of magnesium are detected at the periphery of the material (Fig. 9d). Silicon is mainly observed in the core of the grains. A calcium phosphate-rich layer is formed on the periphery of the grains (Fig. 9b and c). This ability to develop quickly in solution a phosphocalcic layer at the periphery of the material is indicative of its bioactivity. After a few days, the Ca–P layer is almost completely dissolved (data not shown).

For Sr-doped glass, the behaviour is different. After 1 h the dissolution of the glass has hardly begun. No phosphorus is detected around the grains. Only after 1 day of interaction is a uniform Ca–P layer clearly observed at the periphery of the grains. Contrary to the undoped glass, the phosphocalcic layer is not dissolved after 4 days. Some magnesium and strontium are incorporated in the Ca–P layer. The hydroxyapatite being the more stable Ca–P phase at physiological pH, these results are in favour of the formation of an apatitic layer in the case of the doped sample. This is confirmed by quantitative analyses as shown in Fig. 10 where the Ca/P ratio in the periphery of the grains is plotted as a function of immersion time. The exponential like decrease of the Ca/P ratio is much quicker for the Sr-doped glass and the asymptotic value is close to the value of pure HAP (1.67) instead of 2 for the undoped glass.

Finally, ICP-AES titration of the solution after interaction confirms the above mentioned analysis and also demonstrates a partial release of strontium (Fig. 11). The amount of released strontium in physiological conditions is in the order of 11 ppm which is an interesting quantity for osteoporosis treatment.

In conclusion, the superior bioactivity of Sr-doped binary glasses has been demonstrated in vitro. The doped glass reacts more slowly than its undoped counterpart but the Ca–P layer which is formed is much more stable and closer to the composition of HAP phase. Furthermore, in biological conditions, this material is able to release Sr^{2+} ions at an interesting level in the view of treatment of osteoporosis.

In conclusion, sol–gel chemistry appears to be a valuable way to improve the properties of bioceramics by controlled chemical doping. Two new materials have been prepared

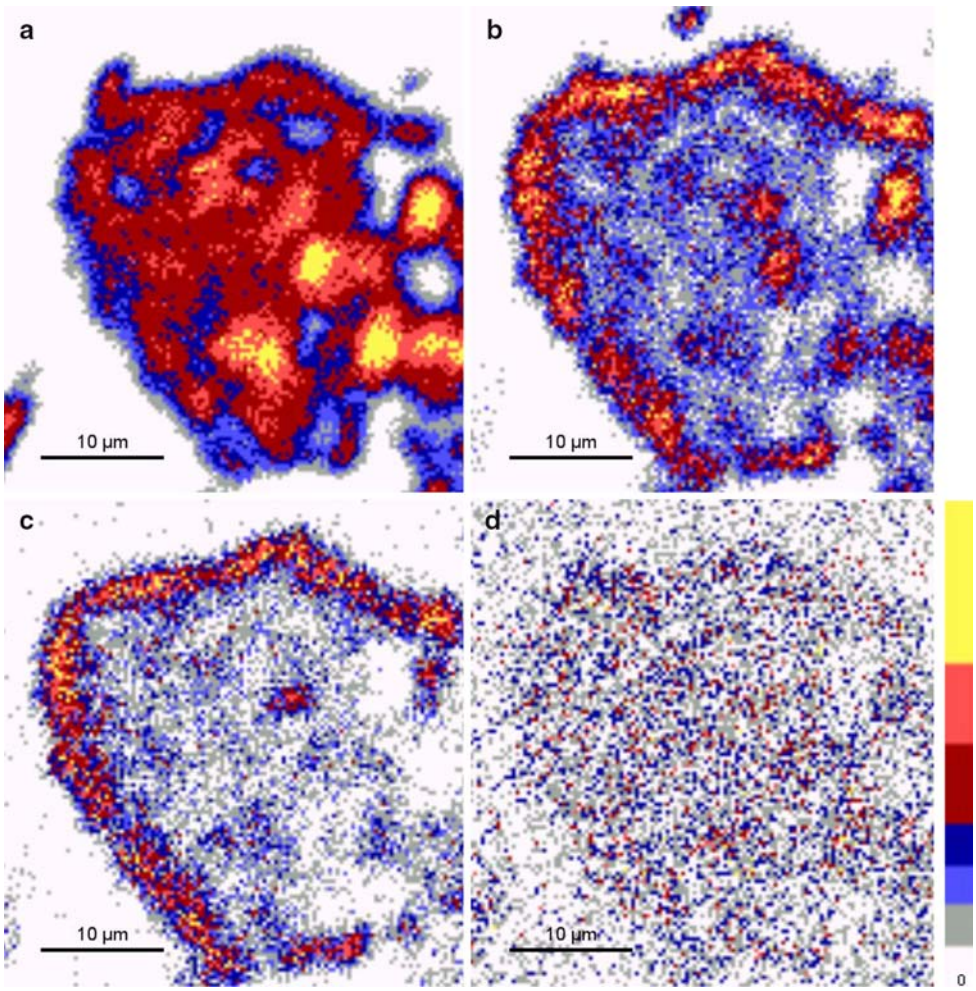

Fig. 9 PIXE elemental maps of a 75 wt% SiO_2–25 wt%CaO glass after 1 h of interaction with biological fluids. (**a**) Silicon, (**b**) calcium, (**c**) phosphorus and (**d**) magnesium

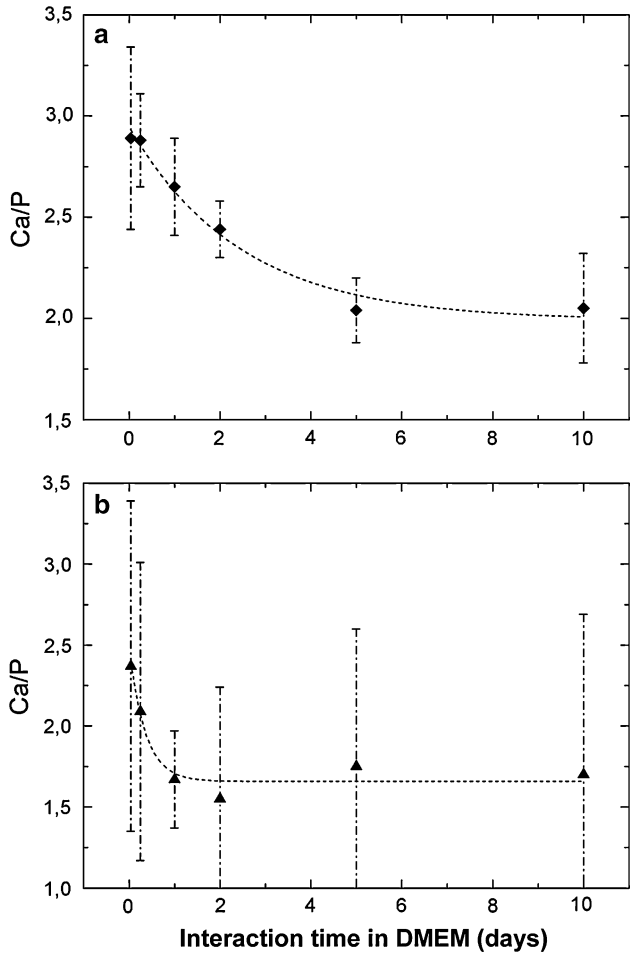

Fig. 10 Evolution of the Ca/P atomic ratio for undoped glass (**a**) and Sr-doped glass (**b**) as a function of interaction time in DMEM

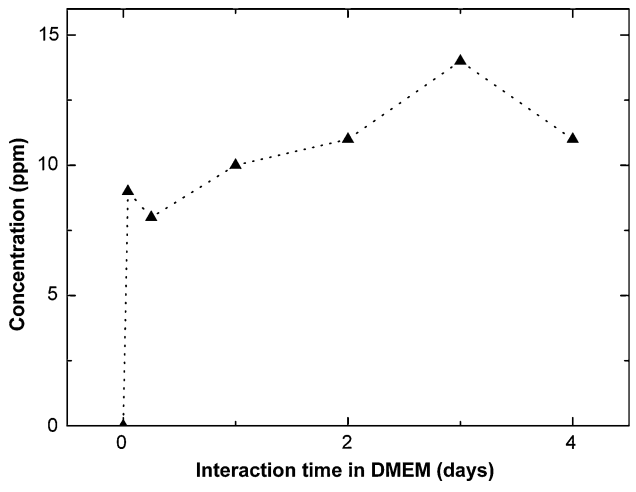

Fig. 11 Evolution of the concentration of released strontium in the biological medium as a function of interaction time for Sr-doped glass

which exhibit interesting in vitro behaviour for the control of inflammatory reactions during surgical operation and for the treatment of osteoporosis during bone substitution.

6 Conclusions

Through various examples taken from our recent work, we have tried to underline the great potentiality of sol–gel chemistry for the preparation of doped materials with good control of doping conditions. In some cases unexpected modification of the materials structure and properties have been observed. Deep understanding of the effects of doping are made possible through systematic studies varying the nature and the concentration of the doping species. This approach can allow the development of new materials with interesting functional properties. The two examples with bioactive ceramics are a good illustration of this point. These two materials have been recently patented owing to their potential use in biomedical systems.

Sol–gel chemistry is widely recognized as a tremendous tool for the preparation of materials with fine control over the structure, morphology and function in particular when coupled with template techniques. This aspect opens the way towards the design of materials with custom-made characteristics. We believe that doping through sol–gel chemistry is a very interesting way to finely tune materials properties. The infinity of possible doping elements makes this issue an open research area.

Acknowledgements The work described in this paper spread over the last 10 years and could have not been possible without numerous collaborations. Among them, the authors would like to thank particularly M. Bouazaoui and B. Capoen from University of Lille, M. Ferrari from CNR Trento, L. L. Hench from Imperial College and R. Mahiou from University of Clermont-Ferrand. Financial support from the French FNS under project LuNaTIC (ACI Nanostructures) and ANR under project Bioverres (PNANO 2005) and Nanobonefiller (PNANO 2006) is gratefully acknowledged.

References

1. (a) Sze SM, Ng Kwok K (2006) Physics of semiconductor devices, 3rd edn. Wiley, New York; (b) Yu PY, Cardona M (2004) Fundamentals of semiconductors: physics and materials properties. Springer; (c) Schubert EF (1993) Doping in III–V semiconductors. Cambridge University Press
2. Blasse G, Grabmaier BC (1994) Luminescent materials. Springer-Verlag
3. (a) (1992) Proc. of heavy scintillators for scientific and industrial applications, Chamonix, France. Edition Frontiere; (b) (1994) Proc. Symp. scintillator and phosphor materials. Materials Research Society, Pittsburgh, 348; (c) (1995) Proc. of inorganic scintillators and their applications. Delft University Press, Delft, Netherlands; (1997) Shangaï Branch Press, Shangaï China; (1999) Moscow, Russia; (2001) Chamonix, France; (2003) Valencia, Spain
4. (a) Holl I, Lorenz E, Mageras G (1988) IEEE Trans Nucl Sci 35(1):105–109; (b) Grabmaier BC (1984) IEEE Trans Nucl Sci 31(1):372–376; (c) Brooks FD (1979) Nucl Inst Methods 162(1–3):477–505; (d) Moszynski M, Kapusta M, Mayhugh M et al (1997) IEEE Trans Nucl Sci 44(3):1052–1061; (e) van Eijk CWE (2001) Nucl Inst Methods Phys Res A 460(1):1–14; (f) Derenzo

SE, Moses WW, Cahoon JL et al (1990) IEEE Trans Nucl Sci 37(2):203–208
5. Melcher CL, Schweitzer JS (1992) Nucl Instrum Methods Phys Res A 314:212
6. Melcher CL, Schweitzer JS U.S. Patents 4,958,080; 5,-025,151; 5,660,627
7. Mansuy C, Nedelec JM, Mahiou R (2004) J Mater Chem 14:3274–3280
8. Mansuy C, Mahiou R, Nedelec JM (2003) Chem Mat 15(17):3242–3244
9. Gustafsson T, Klintenberg M, Derenzo SE, Weber MJ, Thomas JO (2001) Acta Cryst C 57:668
10. Mansuy C, Leroux F, Mahiou R, Nedelec JM (2005) J Mat Chem 15(38):4129–4135
11. Nedelec JM, Mansuy C, Mahiou R (2003) J Mol Struct 651–653C:165–170
12. Mansuy C, Nedelec JM, Dujardin C, Mahiou R (2006) J Sol–Gel Sci Technol 38(1):97–105
13. Mansuy C, Nedelec JM, Dujardin C, Mahiou R (2004) J Sol–Gel Sci Technol 32:253–258
14. Mansuy C, Nedelec JM, Dujardin C, Mahiou R (2007) Opt Mat 29:697–702
15. Mansuy C, Tomasella E, Gengembre L, Grimblot J, Mahiou R, Nedelec JM (2006) Thin Solid Films 515:666–669
16. Nedelec JM, Avignant D, Mahiou R (2002) Chem Mat 14:651
17. Böhlhoff R, Bambauer U, Hoffmann W (1971) Zietschrift fur Kritallographie 133:386
18. Meyer HJ (1972) Naturwissenschaften 59:215
19. Levin EM, Roth RS, Martin JB (1961) Am Mineral 46:1030
20. Boyer D, Bertrand-Chadeyrond G, Mahiou R, Lou L, Brioude A, Mugnier J (2001) Opt Mat 15:21–27
21. Rodriguez-Carvajal J (2004) PROGRA*M FullProf.2k*—version 3.20, Laboratoire Léon Brillouin (CEA-CNRS), France, 2005 (FullProf.2k manual available on http://www-llb.cea.fr/fullweb/fp2k/fp2k_divers.htm). See also J. Rodriguez-Carvajal, T. Roisnel, EPDIC-8, 23–26 May 2002, Trans. Tech. Publication Ltd, Uppsala, Sweden, Mater Sci Forum 123:443
22. Rousset JL, Duval E, Boukenter A, Champagnon B, Monteil A, Serughetti J, Dumas J (1988) J Non-Cryst Solids 107:27
23. Matos MC, Ilharco LM, Almeida RM (1992) J Non-Cryst Solids 147–148:232
24. Abidi N, Deroide B, Zanchetta JV, Bourret D, Elmkami H, Rumori P (1996) Phys Chem Glasses 37(4):149
25. Menassa PE, Simkin DJ, Taylor P (1986) J Lumin 35:223
26. Levy D, Reisfeld R, Avnir D (1984) Chem Phys Lett 109:593
27. Ferrari M, Campostrini R, Carturan G, Montagna M (1992) Philos Mag B 65:251
28. Kinowski C, Turrell S, Bouazaoui M, Capoen B, Nedelec JM, Hench LL (2004) J Sol–Gel Sci Technol 32:345–348
29. Kinowski C, Bouazaoui M, Bechara R, Hench LL, Nedelec JM, Turrell S (2001) J Non-Cryst Solids 291:143
30. Galeener FL (1979) Phys Rev B 19(8):4292
31. Galeener FL, Mikkelsen JC Jr (1981) Phys Rev B 23(10):5527
32. Barrio RA, Galeener FL, Martinez E, Elliott RJ (1993) Phys Rev B 48(21):15672
33. Bertoluzza A, Fagnano C, Morelli MA (1982) J Non-Cryst Solids 48:117
34. Boukenter A, Duval E (1998) Phil Mag B 77(2):557
35. Nedelec JM, Bouazaoui M, Turrell S (1999) J Non-Cryst Solids 243:209
36. Kinowski C, Capoen B, Hench LL, Nedelec J-M, Bechara R, Turrell S, Bouazaoui M (2004) J Non-Cryst Solids 345–346:570–574
37. Nedelec JM, Bouazaoui M, Turrell S (1999) Phys Chem Glasses 40:264
38. Robbe O, Woznica K, Berrier E, Ehrhart G, Capoen B, Bouazaoui M, Turrell S (2006) Thin Solid Films 515(1):73–79
39. Nedelec JM, Capoen B, Turrell S, Bouazaoui M (2001) Thin Solid Films 382:81
40. Berrier E, Capoen B, Bouazaoui M (2005) Glass Technol 46(2):89–93
41. Trimmel G, Schubert U (2001) J Non-Cryst Solids 296:188–200
42. Hench LL, Splinter RJ, Greenlee TK, Allen WC (1971) J Biomed Mater Res 2:117
43. Hench LL (1998) J Am Ceram Soc 81(7):1705–1728
44. Degroot K (1980) Biomaterials 1(1):47–50
45. Ducheyne P (1987) J Biomed Mat Res 21(A2):219–236
46. Doremus RH (1992) J Mat Sci 27(2):285–297
47. Li R, Clark AE, Hench LL (1991) J Appl Biomater 2:231
48. Lao J, Nedelec JM, Moretto P, Jallot E (2006) Nucl Intrum Methods B 245/2:511–518
49. Lao J, Nedelec JM, Moretto P, Jallot E (2007) Nucl Instrum Methods B 261:488–493
50. Bloebaum RD, DuPont JA (1993) J Arthroplasty 8:195–202
51. Bloebaum RD, Beeks J, Dorr LD, Savory CG, DuPont JA, Hofmann AA (1994) Clin Orthop 298:19–26
52. Laquerriere P, Grandjean-Laquerriere A, Jallot E, Balossier G, Frayssinet P, Guenounou M (2003) Biomaterials 24:2739–2747
53. Grandjean-Laquerriere A, Laquerriere P, Laurent-Maquin D, Guenounou M, Phillips TM (2004) Biomaterials 25(28):5921–5927
54. Trindade MCD, Lind M, Nakashima Y, Sun D, Goodman SB, Schurman DJ, Smith RL (2001) Biomaterials 22:2067–2073
55. Yamaguchi M, Inamoto K, Suketa Y (1986) Res Exp Med 186(5):337–342
56. Hashizume M, Yamaguchi M (1993) Mol Cell Biochem 122(1):59–64
57. Kishi S, Yamaguchi M (1994) Biochem Pharmacol 48(6):1225–1230
58. Bao B, Prasad AS, Beck FW, Godmere M (2003) Am J Physiol Endocrinol Metab 285(5):1095
59. Jallot E, Nedelec JM, Grimault AS, Chassot E, Laquerriere P, Grandjean-Laquerriere A, Laurent-Maquin D (2005) Colloids Surf B 42:205–210
60. Grandjean-Laquerriere A, Laquerriere P, Jallot E, Nedelec JM, Guenounou M, Laurent-Maquin D, Philips T (2006) Biomaterials 27:3195–3200
61. Laquerriere P, Grandjean-Laquerriere A, Jallot E, Nedelec J-M A Zn-substituted hydroxyapatite with reduced inflammatory properties and uses thereof. (US 60/751,977)
62. Meunier PJ, Lorenc RS, Smith IG (2002) Osteoporos Int 13(3):66
63. Marie PJ (2005) Curr Opin Pharmacol 5:633–636
64. Jensen JEB, Stang H, Kringsholm B (1997) Bone 20(4):104–108